



Stellar Metallicities and Elemental Abundance Ratios of $z \sim 1.4$ Massive Quiescent Galaxies*

Mariska Kriek¹ , Sedona H. Price² , Charlie Conroy³ , Katherine A. Suess¹ , Lamiya Mowla⁴ , Imad Pasha⁴ ,
Rachel Bezanson⁵ , Pieter van Dokkum⁴, and Guillermo Barro⁶

¹Astronomy Department, University of California, Berkeley, CA 94720, USA

²Max Planck Institute for Extraterrestrial Physics, Giessenbachstrasse 1, D-85741 Garching, Germany

³Harvard-Smithsonian Center for Astrophysics, 60 Garden Street, Cambridge, MA, USA

⁴Department of Astronomy, Yale University, New Haven, CT 06511, USA

⁵Department of Physics and Astronomy and PITT PACC, University of Pittsburgh, Pittsburgh, PA, 15260, USA

⁶Department of Physics, University of the Pacific, 3601 Pacific Avenue, Stockton, CA 95211, USA

Received 2019 March 25; revised 2019 July 1; accepted 2019 July 2; published 2019 August 1

Abstract

The chemical composition of galaxies has been measured out to $z \sim 4$. However, nearly all studies beyond $z \sim 0.7$ are based on strong-line emission from H II regions within star-forming galaxies. Measuring the chemical composition of distant quiescent galaxies is extremely challenging, as the required stellar absorption features are faint and shifted to near-infrared wavelengths. Here, we present ultradeep rest-frame optical spectra of five massive quiescent galaxies at $z \sim 1.4$, all of which show numerous stellar absorption lines. We derive the abundance ratios [Mg/Fe] and [Fe/H] for three out of five galaxies; the remaining two galaxies have too young luminosity-weighted ages to yield robust measurements. Similar to lower-redshift findings, [Mg/Fe] appears positively correlated with stellar mass, while [Fe/H] is approximately constant with mass. These results may imply that the stellar mass–metallicity relation was already in place at $z \sim 1.4$. While the [Mg/Fe]–mass relation at $z \sim 1.4$ is consistent with the $z < 0.7$ relation, [Fe/H] at $z \sim 1.4$ is ~ 0.2 dex lower than at $z < 0.7$. With a [Mg/Fe] of $0.44^{+0.08}_{-0.07}$ the most massive galaxy may be more α -enhanced than similar-mass galaxies at lower redshift, but the offset is less significant than the [Mg/Fe] of 0.6 previously found for a massive galaxy at $z = 2.1$. Nonetheless, these results combined may suggest that [Mg/Fe] in the most massive galaxies decreases over time, possibly by accreting low-mass, less α -enhanced galaxies. A larger galaxy sample is needed to confirm this scenario. Finally, the abundance ratios indicate short star formation timescales of 0.2–1.0 Gyr.

Key words: galaxies: evolution – galaxies: formation

1. Introduction

The chemical composition of a galaxy reflects the interplay of several fundamental physical processes in galaxy formation, including star formation, metal production, feedback and gas exchange with the surrounding medium, and galaxy merging. Subsequent star formation episodes and the recycling of enriched gas result in an increase of metallicity with time, while the duration of the star-forming phase sets the relative abundances of different metals. Feedback processes further impact the chemical enrichment history, as they may expel enriched gas from galaxies. In combination with inflow of lower-metallicity gas from the inter/circumgalactic medium, they alter the metal content of the gas supply. Finally, galaxy mergers affect the chemical composition, as stars in accreted galaxies have their own chemical footprint (see Maiolino & Mannucci 2019 and references therein).

Metallicities of low-redshift galaxies have been studied extensively for both the interstellar gas (e.g., Tremonti et al. 2004) as well as the gas locked up in stars (e.g., Gallazzi et al. 2005). To disentangle the effects of star formation, feedback/gas exchange, and galaxy mergers on the chemical abundance

patterns of galaxies, it is crucial to extend these studies to higher redshifts. Metallicities of star-forming galaxies have been studied out to $z \sim 4$ (e.g., Erb et al. 2006; Mannucci et al. 2009; Shapley et al. 2017). However, the chemical composition of quiescent galaxies has only been routinely measured out to $z \sim 0.7$ (e.g., Choi et al. 2014; Gallazzi et al. 2014). Because quiescent galaxies dominate the massive galaxy population out to $z \sim 2$ (Muzzin et al. 2013b; Tomczak et al. 2014), our current understanding of the chemical composition of galaxies through cosmic time is thus incomplete.

Measuring chemical compositions of $z > 0.7$ quiescent galaxies is extremely challenging as the required stellar absorption lines are faint and shifted to near-infrared wavelengths. Furthermore, because of the younger stellar ages, the metal absorption lines for distant quiescent galaxies are weaker than for their local analogs. The few available measurements at $z > 0.7$ are either based on a stacked spectrum of quiescent galaxies (e.g., Onodera et al. 2015), or on an ultradeep spectrum of a single quiescent galaxy (e.g., Toft et al. 2012; Lonoce et al. 2015; Kriek et al. 2016). There are also several studies that use low-resolution grism spectra obtained with the *Hubble Space Telescope* (*HST*) to derive stellar metallicities (e.g., Estrada-Carpenter et al. 2019; Morishita et al. 2018). However, because these studies primarily rely on the continuum shape, they are especially susceptible to modeling degeneracies and other systematic errors.

* Based on data obtained at the W.M. Keck Observatory and with the NASA/ESA *Hubble Space Telescope* (*HST*). W.M. Keck Observatory is operated as a scientific partnership among the California Institute of Technology, the University of California and NASA, and was made possible by the generous financial support of the W.M. Keck Foundation. *HST* is operated by the Association of Universities for Research in Astronomy, Inc., under NASA contract NAS 5-26555.

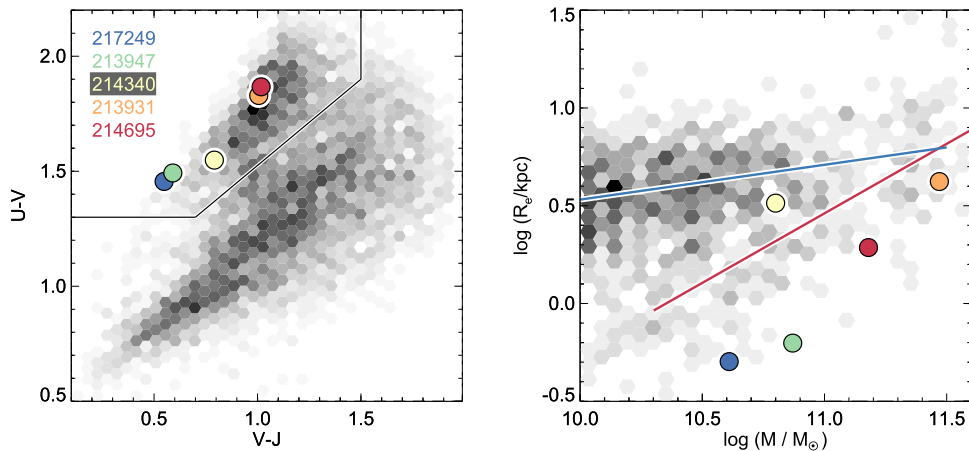


Figure 1. Left: rest-frame $U - V$ vs. $V - J$ of the five quiescent galaxies observed with MOSFIRE and LRIS in comparison to all galaxies with $1.3 < z < 1.5$ and $\log(M/M_\odot) > 10$ in the UltraVISTA field. Right: rest-frame optical size (at 5000 \AA) vs. stellar mass of the same five galaxies in comparison to all galaxies with $1.3 < z < 1.5$ and $\log(M/M_\odot) > 10$ from Mowla et al. (2018). The blue and red lines represent the best-fit relations for star-forming and quiescent galaxies, respectively, at $z \sim 1.4$ (Mowla et al. 2018). The most massive galaxy, 213931, consists of three clumps. In this panel we show the size and mass of the brightest clump, where the mass has been estimated using the magnitude ratios of the clumps.

Early results suggest that $z > 0.7$ quiescent galaxies have supersolar metallicities (Lonoce et al. 2015; Onodera et al. 2015; Kriek et al. 2016) and are α -enhanced with $[\text{Mg}/\text{Fe}]$ that are similar (Onodera et al. 2015) or significantly higher (Lonoce et al. 2015; Kriek et al. 2016) than those of similar-mass low-redshift galaxies. These high $[\text{Mg}/\text{Fe}]$ imply very short star formation timescales, though the stellar initial mass function (IMF) may also affect this abundance ratio (e.g., Fontanot et al. 2017). Furthermore, these measurements raise the question of how high-redshift quiescent galaxies with high $[\text{Mg}/\text{Fe}]$ evolve into the early-type galaxy population with lower $[\text{Mg}/\text{Fe}]$ seen today. Larger galaxy samples are needed to confirm these results.

In this Letter we present elemental abundance ratios for five massive galaxies at $z \sim 1.4$, derived from deep spectra obtained with LRIS and MOSFIRE on the Keck I Telescope. This study is enabled by the large UltraVISTA (McCracken et al. 2012) and COSMOS-DASH (Momcheva et al. 2017; Mowla et al. 2018) field, which facilitated the identification of pointings for which we can observe several bright targets (with *HST*/F160W imaging) simultaneously. Throughout this work we assume a Λ CDM cosmology with $\Omega_m = 0.3$, $\Omega_\Lambda = 0.7$, and $H_0 = 70 \text{ km s}^{-1} \text{ Mpc}^{-1}$.

2. Galaxy Sample and Data

The observed galaxies were identified using the UltraVISTA *K*-band selected catalog (v4.1) by Muzzin et al. (2013a). We selected the pointing for which we could observe the most $J < 21.6$ quiescent galaxies at $1.3 < z < 1.5$ in one MOSFIRE/LRIS mask. For this redshift range, we catch prominent metal and Balmer absorption lines in atmospheric windows. Galaxies were classified as quiescent based on their rest-frame $U - V$ and $V - J$ colors (e.g., Wuyts et al. 2007). Furthermore, we required that the pointing overlaps with the COSMOS-DASH survey (Momcheva et al. 2017; Mowla et al. 2018), which provides shallow F160W imaging and thus allows the measurement of rest-frame optical sizes. Figure 1 shows the location of the five targets in the rest-frame $U - V$ versus $V - J$ (UVJ) diagram, as well as in R_e versus stellar mass space, compared to the full galaxy distribution with $M > 10^{10} M_\odot$ and $1.3 < z < 1.5$ (Muzzin et al. 2013b; Mowla et al. 2018). The galaxies span a range in colors along the

quiescent sequence in the UVJ diagram, as well as a range in sizes. On average, they are slightly bluer and smaller than the typical quiescent galaxy at this redshift. This bias may be expected; our magnitude selection favors post-starburst galaxies, which are brighter, bluer, and presumably smaller than older quiescent galaxies of similar mass (e.g., Whitaker et al. 2012; Yano et al. 2016; Almaini et al. 2017).

The LRIS mask containing our five primary targets was observed for ~ 4.5 hr on 2017 January 4 using the 600/10,000 red grating, $1''$ -wide slits, and an ABC dither pattern. The sky was clear with an image quality of $\sim 0''.8$ – $1''.0$. The same five galaxies were observed within one MOSFIRE mask on 2017 March 15 and April 5–6 for ~ 12 hr in *J*, using $0''.7$ -wide slits and an ABA'B' dither pattern (Kriek et al. 2015). The sky was clear and the seeing varied between $0''.5$ and $1''.0$. For both instruments we assigned a star to one of the slits to monitor weather conditions and aid the data reduction.

The LRIS and MOSFIRE 2D spectra were reduced using custom software. Initial sky subtraction was performed using the average of the surrounding frames with the same integration times. Cosmic rays were identified using L.A. Cosmic (van Dokkum 2001) and combined with a bad pixel map. Next, the individual sky-subtracted frames and corresponding masks were resampled onto a common grid to account for the wavelength calibration, dither position, distortions, and drifts. An additional sky subtraction was performed by subtracting the median background at each wavelength. For the MOSFIRE spectra, the slit stars were used to derive a weighing factor for each science exposure. All LRIS frames were weighted equally, since the weather conditions were stable.

The individual spectra were average combined, taking into account both the weighing factors and the corresponding rectified masks. The relative flux calibration was performed using a response spectrum. For MOSFIRE the response spectrum was derived from the spectra of A0 V stars. For LRIS we used the theoretical atmospheric absorption spectrum, adjusted to match the atmospheric features in the spectrum of the slit star, combined with the intrinsic shape of the slit star and other bright objects in the mask. More details on the MOSFIRE reduction software, which was developed for the MOSDEF survey, are given in Kriek et al. (2015). One-dimensional (1D) spectra were extracted

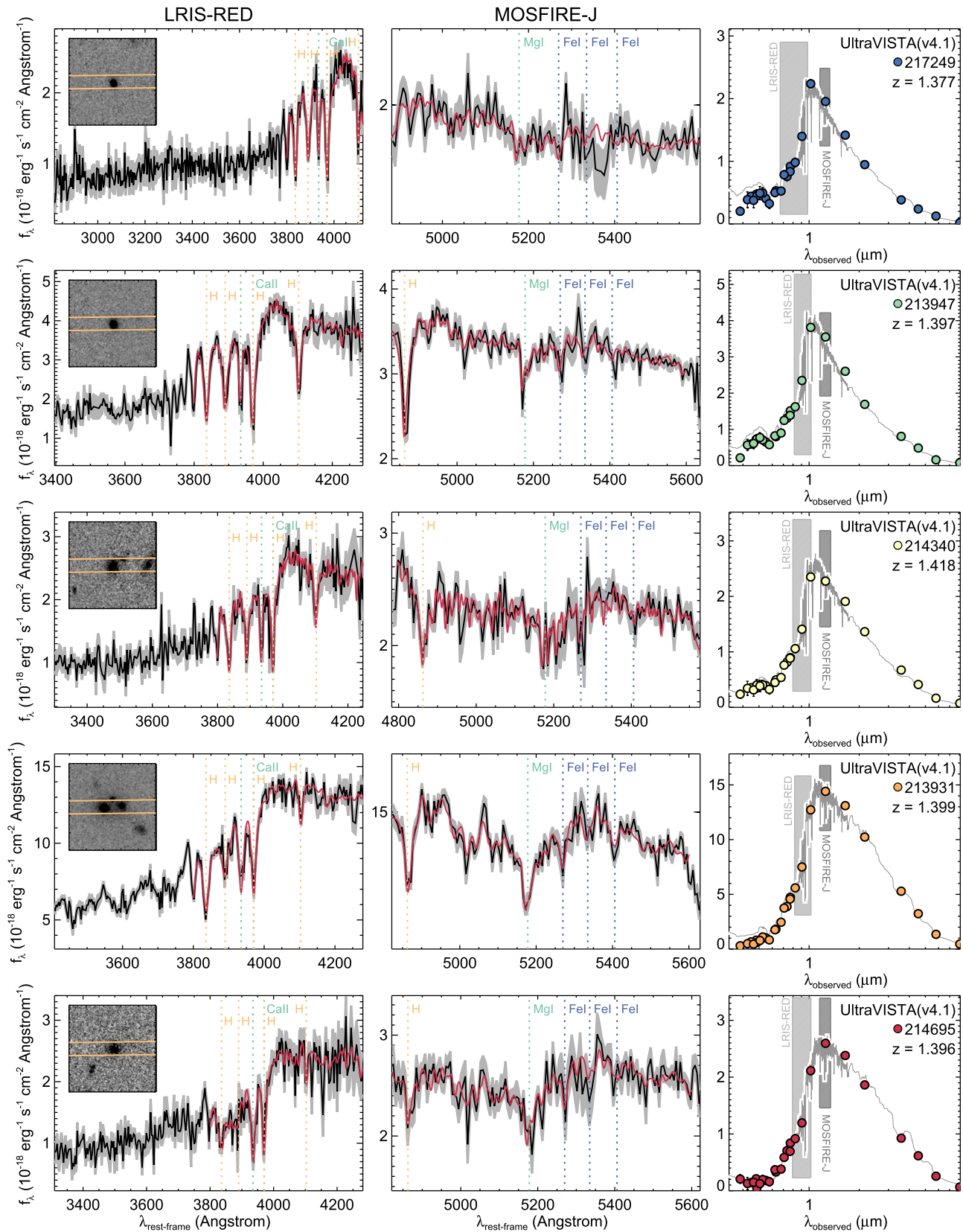


Figure 2. Left: LRIS-RED and MOSFIRE/*J*-band spectra of five massive quiescent galaxies at $z \sim 1.4$ (black). The spectra are binned by 10 pixels, corresponding to ~ 3.3 and ~ 5.4 rest-frame \AA per bin for the LRIS and MOSFIRE spectra, respectively. The gray areas represent the 1σ uncertainty for the binned spectra. The best-fit $a1f$ models are shown in red. The F814W image ($4''.5 \times 4''.5$) is shown in the inset, with the MOSFIRE slit overplotted (91° , $0''.7$ width). The LRIS slit had a similar orientation (93°) and width ($1''$). Right: UltraVISTA photometry (circles) and best-fit FSPS model (gray) for the same galaxies.

using an optimal weighing procedure. The combined LRIS and MOSFIRE spectra for each galaxy, together with the *HST* F814W image (Scoville et al. 2007) and the photometric spectral energy distribution (Muzzin et al. 2013b), are shown in Figure 2. We detect numerous stellar absorption lines for all five galaxies.

The most massive galaxy in the sample, 213931, consists of three separate clumps, which were blended together as one system in the UltraVISTA images and catalog. As illustrated in Figure 2, the slit was aligned along the two most massive clumps. With MOSFIRE we detect two blended traces, though one of the traces is significantly fainter, and no separate analysis could be performed. Using LRIS, we do not detect two separate traces, and thus we treat 213931 as one system in our analysis.

3. Analysis

We use the absorption line fitter (`alf`) code to estimate parameters from the combined 1D LRIS and MOSFIRE spectra. The code is described in detail in Conroy & van Dokkum (2012), Conroy et al. (2014), and Choi et al. (2014). In summary, `alf` combines libraries of isochrones and empirical stellar spectra with synthetic stellar spectra covering a wide range of elemental abundance patterns. The code fits for C, N, O, Na, Mg, Ca, Ti, V, Cr, Mn, Fe, Co, and Ni abundances, redshift, velocity dispersion, stellar population age, and several emission lines. The ratio of the model and data is fit by a high-order polynomial in order to avoid potential issues with the flux calibration of the data. The fitting is done using a Markov Chain Monte Carlo (MCMC) algorithm (Foreman-Mackey et al. 2013). This spectral modeling approach is strongly preferred over the use of integrated absorption line measurements for distant galaxies (see the discussion in Kriek et al. 2016).

For our $z \sim 1.4$ galaxies, we assume the Kroupa (2001) IMF and allow for a double-component stellar population with two different ages. This model is preferred over a single-age model (i.e., SSP), because it indirectly separates the younger and older stellar populations and results in mass-weighted abundance measurements. In case we assume an SSP, the younger stars will disproportionately dominate the results. In Table 1 we list mass-weighted abundance ratios and ages for the double-component model, as well as the ages for an SSP. Due to the mass weighing, the double-component ages are older than the SSP ages (which are closer to luminosity-weighted ages). While all abundances are free parameters, only few can be accurately determined. We also determine the total stellar metallicity using $[Z/H] = [Fe/H] + 0.94[Mg/Fe]$ (Thomas et al. 2003), and derive the 16% and 84% confidence intervals from the $[Z/H]$ distribution following from the MCMC simulations.

Stellar masses are derived by fitting the combined continuum spectra and UltraVISTA photometry with the Flexible Stellar Population Synthesis (FSPS) models (Conroy et al. 2009), using the FAST fitting code (Kriek et al. 2009). We assume solar metallicity, a delayed exponential star formation history, the Chabrier (2003) IMF, and the average attenuation law by Kriek & Conroy (2013). We caution though that these stellar masses are likely underestimated, and more complicated star formation histories, like the one assumed in the `alf` fitting, would lead to masses that are $\sim 50\%$ larger.

Table 1
Parameters of $z \sim 1.4$ Quiescent Galaxies

ID ^a	FAST $\log M$ M_{\odot}	alf				
		σ_v (km s^{-1})	[Fe/H]	[Mg/Fe]	t (Gyr)	t_{SSP} (Gyr)
217249	10.61	127^{+58}_{-29}	$-1.03^{+0.47}_{-0.27}$	$0.52^{+0.28}_{-0.35}$	$3.0^{+0.4}_{-0.6}$	$0.9^{+0.8}_{-0.4}$
213947	10.87	170^{+25}_{-19}	$-0.89^{+0.68}_{-0.24}$	$0.57^{+0.24}_{-0.32}$	$3.0^{+0.1}_{-1.0}$	$0.8^{+0.2}_{-0.3}$
214340	10.80	79^{+24}_{-27}	$-0.42^{+0.16}_{-0.24}$	$0.22^{+0.19}_{-0.14}$	$3.8^{+5.3}_{-0.8}$	$1.4^{+0.6}_{-0.5}$
213931 ^b	11.73	342^{+12}_{-11}	$-0.27^{+0.07}_{-0.07}$	$0.44^{+0.08}_{-0.07}$	$3.1^{+0.2}_{-0.1}$	$2.0^{+0.8}_{-0.5}$
214695	11.18	209^{+30}_{-33}	$-0.20^{+0.17}_{-0.22}$	$0.28^{+0.15}_{-0.14}$	$4.5^{+2.9}_{-1.2}$	$3.8^{+7.3}_{-1.6}$

Notes.

^a UltraVISTA catalog v4.1 by Muzzin et al. (2013a).

^b The mass for this galaxy represents the total mass, including all three clumps.

Rest-frame optical sizes are derived from the combination of F814W data from Scoville et al. (2007) and F160W data from COSMOS-DASH, following the procedure described in Mowla et al. (2018). This procedure relies on Sérsic fits and the GALFIT modeling code (Peng et al. 2002). We derive the (noncircularized) size at 5000 Å using a linear interpolation between the F814W and F160W sizes. For 213931, we measure the size of the brightest clump.

4. Results

In Figure 3, we show the abundance ratios $[Mg/Fe]$ and $[Fe/H]$ of the $z \sim 1.4$ galaxies in comparison with galaxies at lower redshift (Conroy & van Dokkum 2012; Choi et al. 2014) and a single massive quiescent galaxy at $z = 2.1$ (Kriek et al. 2016). Although metal and Balmer absorption lines are detected for all five galaxies, the abundance ratios for 217249 and 213947 are poorly constrained. Figures 1 and 2 show that these galaxies have blue rest-frame colors, strong Balmer lines, and are dominated by A-type stars. Hence, their luminosity-weighted ages are relatively young, and thus their metal lines are weak. Therefore, in Figure 3 we only show the three redder quiescent galaxies at $z \sim 1.4$. For these galaxies we find similar abundance ratios when adopting a single-age model.

In the left panels of Figure 3, we show the abundance ratios $[Mg/Fe]$ and $[Fe/H]$ versus stellar mass. We compare our results to the work by Choi et al. (2014), based on stacked spectra of quiescent galaxies at $0.07 < z < 0.7$. In the right panels we show the abundance ratios as a function of the observed integrated stellar velocity dispersion (σ_v), in comparison to the nearby early-type galaxy sample by Conroy & van Dokkum (2012). All abundance ratios and velocity dispersions have been derived using the `alf` code. However, stellar masses and velocity dispersions were not consistently derived for all samples, and thus we only show the comparison samples if the measurements are available.

Similar to $z < 0.7$, $[Mg/Fe]$ appears positively correlated with both stellar mass and σ_v at $z \sim 1.4$. These results, however, are based on only three galaxies; a larger sample is needed to confirm these trends. The two lower-mass galaxies (214340 and 214695) have $[Mg/Fe]$ similar to their lower-redshift analogs. With a $[Mg/Fe]$ of 0.44, the most massive galaxy (213931) is slightly offset from the low-redshift $[Mg/Fe]$ –mass and $[Mg/Fe]$ – σ_v relations. This offset, however, is not significant, and larger galaxy samples are needed to assess whether the most massive galaxies are indeed more α -enhanced at earlier times.

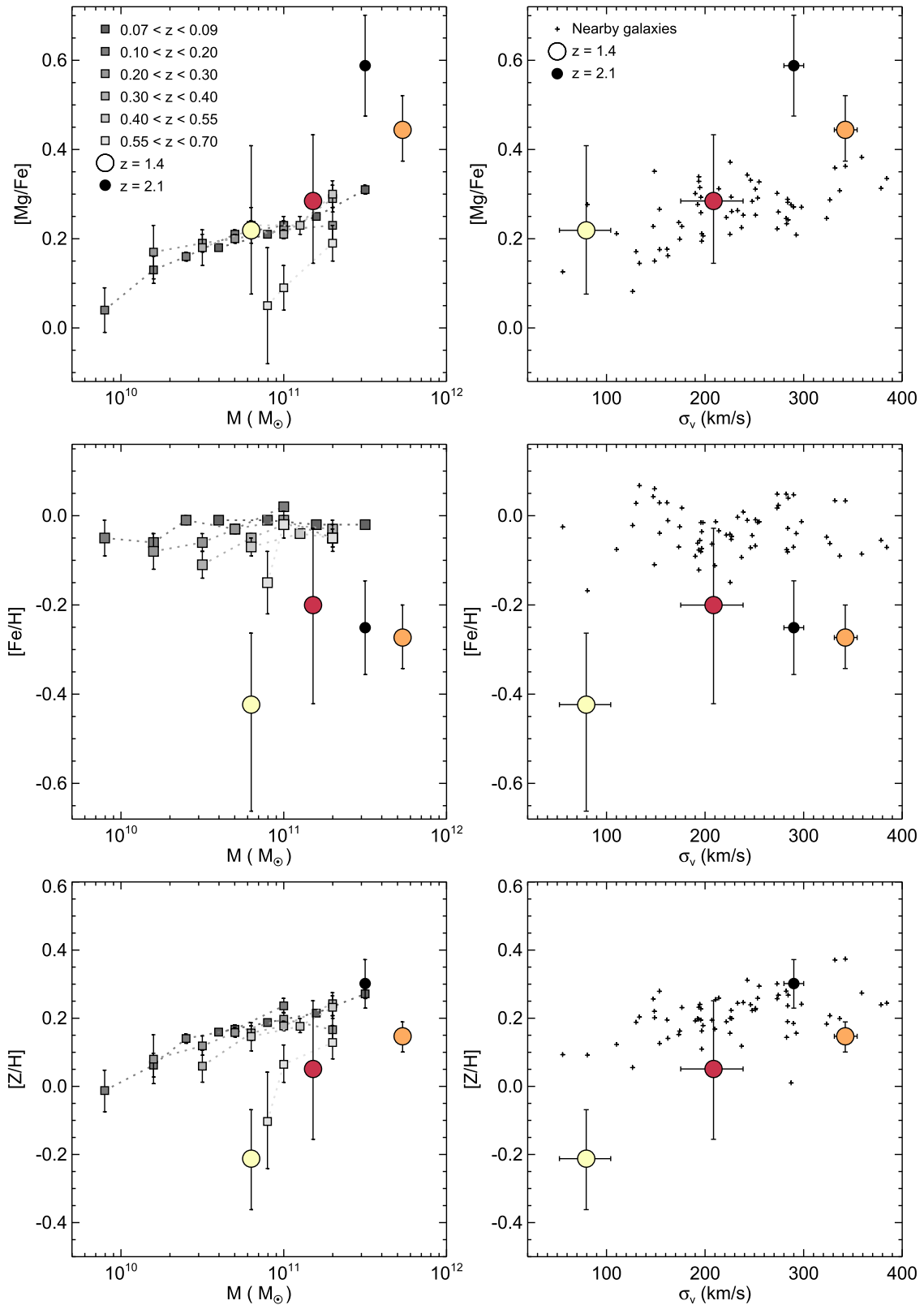


Figure 3. [Mg/Fe] (top), [Fe/H] (middle), and [Z/H] (bottom) vs. stellar mass (left) and velocity dispersion (right) of the $z \sim 1.4$ quiescent galaxies 214340 (yellow), 213931 (orange), and 214695 (red), in comparison to nearby early-type galaxies (pluses; Conroy & van Dokkum 2012), stacks of quiescent galaxies at $0.07 < z < 0.70$ (squares; Choi et al. 2014), and a quiescent galaxy at $z = 2.1$ (black filled circle; Kriek et al. 2016). For all (stacks of) galaxies, the abundance ratios and velocity dispersions were derived using `a1f`. The relations at $z \sim 1.4$ are similar to those at $z < 0.7$, though [Fe/H] seems offset to lower values. The bottom panels show that a tentative stellar mass–metallicity relation may already be in place at $z \sim 1.4$, possibly offset to lower metallicities.

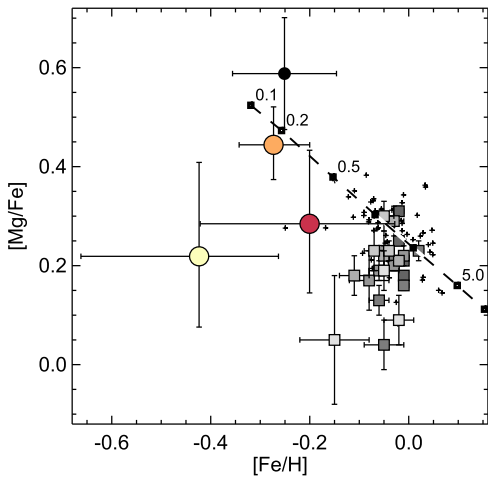


Figure 4. $[\text{Mg}/\text{Fe}]$ vs. $[\text{Fe}/\text{H}]$ for massive quiescent galaxies at $z \sim 1.4$ (colored symbols), in comparison to nearby early-type galaxies (pluses), stacks of quiescent galaxies at $0.07 < z < 0.70$ (gray squares), and a quiescent galaxy at $z = 2.1$ (black filled circle). Symbols are the same as in Figure 3. The dashed line represents a chemical evolution model, with different star formation timescales in Gyr indicated by the small black squares. The abundance ratios of the two most massive galaxies (orange and black circles) at $z \gtrsim 1.4$ suggest that their star formation timescales are shorter than for $z < 0.7$ galaxies.

Similar to the low-redshift samples, we find no correlation between $[\text{Fe}/\text{H}]$ and mass or σ_v . We do find an offset in $[\text{Fe}/\text{H}]$, such that the $z \sim 1.4$ galaxies are deficient in iron compared to similar-mass low-redshift galaxies.

In Figure 4 we compare the combined abundance ratios $[\text{Mg}/\text{Fe}]$ and $[\text{Fe}/\text{H}]$ to a closed-box chemical evolution model for different star formation timescales. This model assumes a Salpeter (1955) IMF, a constant SFR, the core-collapse and Type Ia SN yield models by Kobayashi et al. (2006) and Nomoto et al. (1984), and a Type Ia delay time distribution of the form t^{-1} between 0.1 and 13 Gyr (Maoz et al. 2012). Comparison with this model indicates that the $z \sim 1.4$ galaxies formed their stars over a brief time period of ~ 0.2 –1 Gyr. As discussed in Kriek et al. (2016), by adopting different core-collapse supernova yields or a different Type Ia delay time distribution, we can change this model substantially.

5. Discussion

In this Letter, we present ultradeep rest-frame optical spectra of five massive quiescent galaxies at $z \sim 1.4$, all of which show multiple stellar absorption lines. For three galaxies we derive the abundance ratios $[\text{Mg}/\text{Fe}]$ and $[\text{Fe}/\text{H}]$, but the remaining two galaxies have too young luminosity-weighted ages to yield robust measurements. Similar to $z < 0.7$ studies, we find a tentative positive relation between $[\text{Mg}/\text{Fe}]$ and stellar mass (or velocity dispersion). Also similar to $z < 0.7$, we find no correlation between $[\text{Fe}/\text{H}]$ and stellar mass (or velocity dispersion). Our results may imply that the stellar mass–metallicity relation was already in place at $z \sim 1.4$ (bottom panels of Figure 3).

While the $[\text{Mg}/\text{Fe}]$ –mass relation at $z \sim 1.4$ is consistent with the $z \lesssim 0.7$ relation, $[\text{Fe}/\text{H}]$ at $z \sim 1.4$ is ~ 0.2 dex lower than at $z < 0.7$. We also found a low $[\text{Fe}/\text{H}]$ for a single massive quiescent galaxy at $z = 2.1$ (Kriek et al. 2016). In addition to the low $[\text{Fe}/\text{H}]$, this $z = 2.1$ galaxy was more α -enhanced than low-redshift galaxies of similar mass, with a $[\text{Mg}/\text{Fe}]$ of 0.6. The most massive galaxy in the current sample has a $[\text{Mg}/\text{Fe}]$ of $0.44^{+0.08}_{-0.07}$,

and thus may also be more α -enhanced than lower-redshift analogs. Combined, these results may suggest that $[\text{Mg}/\text{Fe}]$ of the most massive galaxies decreases over cosmic time, possibly by accretion of low-mass, less α -enhanced galaxies.

A similar scenario has been proposed to explain the evolution in the mass–size relation of quiescent galaxies between $z \sim 2$ and $z \sim 0$ (e.g., van Dokkum et al. 2008; Bezanson et al. 2009; Naab et al. 2009). In this context, we note that all three $z \sim 1.4$ galaxies as well as the $z \sim 2.1$ galaxy have close neighbors, and thus may be in the process of merging with smaller galaxies (see also Gu et al. 2018). However, as $[\text{Fe}/\text{H}]$ is constant with mass, it is not obvious how this scenario could increase $[\text{Fe}/\text{H}]$, and a larger galaxy sample is needed to understand the evolutionary scenario (Choi et al. 2014). Other possible scenarios include late-time star formation and the growth of the quiescent galaxy population over time. Galaxies that stop forming stars at later times will have lower $[\text{Mg}/\text{Fe}]$, higher $[\text{Fe}/\text{H}]$, and larger sizes (Khochfar & Silk 2006). Thus, once these galaxies join the quiescent population, they will alter the average size and abundance ratios (e.g., Carollo et al. 2013; Choi et al. 2014).

Our metallicities are higher than the subsolar metallicities found by Morishita et al. (2018) for two $10^{11} M_{\odot}$ quiescent galaxies at $z \sim 2.2$, but lower than the supersolar metallicities found for a stack of massive ($\log M/M_{\odot} \sim 11.4$) galaxies at $z \sim 1.6$ ($[\text{Z}/\text{H}] = 0.24^{+0.20}_{-0.14}$; Onodera et al. 2015), our $z = 2.1$ galaxy ($[\text{Z}/\text{H}] = 0.30 \pm 0.07$; Kriek et al. 2016), as well as the $z \sim 1.4$ galaxy by Lonoce et al. (2015, $[\text{Z}/\text{H}] > 0.5$). Our results are more similar to the solar metallicities found by Estrada-Carpenter et al. (2019) for stacks of $1.0 < z < 1.8$ galaxies ($\log M/M_{\odot} \sim 10.8$). We do caution though that these studies use varying data sets and techniques to measure stellar metallicities, and thus different assumptions and other systematics complicate the comparison.

Larger samples are needed to obtain a full census of the relation between the chemical composition, stellar mass, and structures of distant quiescent galaxies. This work is part of a survey to obtain deep rest-frame optical spectra and elemental abundance measurements for a sample of 20 distant quiescent galaxies; 10 galaxies at $z \sim 1.4$ and 10 galaxies at $z \sim 2.1$. The current study demonstrates that such measurements are only possible for individual quiescent galaxies that are dominated by an older stellar population, which have more pronounced metal lines. For quiescent galaxies that are dominated by a younger stellar population we have to rely on stacking techniques to obtain more robust measurements. In the near future, we will use our full sample to measure the relations between the chemical composition, age, stellar mass/velocity dispersion, and galaxy sizes/structures at $z \sim 1.4$ and $z \sim 2.1$, and compare them to the lower-redshift relations. In the more distant future, NIRSpect on the *James Webb Space Telescope* will enable the first resolved stellar abundance studies at these redshifts. These two studies together, in combination with the resolved stellar abundance studies at low redshift (e.g., Greene et al. 2015), will open a new window into the chemical enrichment, star formation, and assembly histories of massive quiescent galaxies.

We thank the referee for a very thoughtful and constructive report, Ryan Trainor for his help with the LRIS observations, and Jenny Greene and Marijn Franx for valuable discussions. We acknowledge support from NSF AAG grants AST-1908748 and 1909942. The authors wish to recognize and acknowledge the

very significant cultural role and reverence that the summit of Maunakea has always had within the indigenous Hawaiian community. We are most fortunate to have the opportunity to conduct observations from this mountain.

ORCID iDs

Mariska Kriek  <https://orcid.org/0000-0002-7613-9872>
 Sedona H. Price  <https://orcid.org/0000-0002-0108-4176>
 Charlie Conroy  <https://orcid.org/0000-0002-1590-8551>
 Katherine A. Suess  <https://orcid.org/0000-0002-1714-1905>
 Lamiya Mowla  <https://orcid.org/0000-0002-8530-9765>
 Imad Pasha  <https://orcid.org/0000-0002-7075-9931>
 Rachel Bezanson  <https://orcid.org/0000-0001-5063-8254>
 Guillermo Barro  <https://orcid.org/0000-0001-6813-875X>

References

- Almaini, O., Wild, V., Maltby, D. T., et al. 2017, *MNRAS*, 472, 1401
 Bezanson, R., van Dokkum, P. G., Tal, T., et al. 2009, *ApJ*, 697, 1290
 Carollo, C. M., Bschorr, T. J., Renzini, A., et al. 2013, *ApJ*, 773, 112
 Chabrier, G. 2003, *PASP*, 115, 763
 Choi, J., Conroy, C., Moustakas, J., et al. 2014, *ApJ*, 792, 95
 Conroy, C., Graves, G. J., & van Dokkum, P. G. 2014, *ApJ*, 780, 33
 Conroy, C., Gunn, J. E., & White, M. 2009, *ApJ*, 699, 486
 Conroy, C., & van Dokkum, P. G. 2012, *ApJ*, 760, 71
 Erb, D. K., Shapley, A. E., Pettini, M., et al. 2006, *ApJ*, 644, 813
 Estrada-Carpenter, V., Papovich, C., Momcheva, I., et al. 2019, *ApJ*, 870, 133
 Fontanot, F., De Lucia, G., Hirschmann, M., et al. 2017, *MNRAS*, 464, 3812
 Foreman-Mackey, D., Hogg, D. W., Lang, D., & Goodman, J. 2013, *PASP*, 125, 306
 Gallazzi, A., Bell, E. F., Zibetti, S., Brinchmann, J., & Kelson, D. D. 2014, *ApJ*, 788, 72
 Gallazzi, A., Charlot, S., Brinchmann, J., White, S. D. M., & Tremonti, C. A. 2005, *MNRAS*, 362, 41
 Greene, J. E., Janish, R., Ma, C.-P., et al. 2015, *ApJ*, 807, 11
 Gu, M., Conroy, C., & Brammer, G. 2018, *ApJL*, 862, L18
 Khochfar, S., & Silk, J. 2006, *ApJL*, 648, L21
 Kobayashi, C., Umeda, H., Nomoto, K., Tominaga, N., & Ohkubo, T. 2006, *ApJ*, 653, 1145
 Kriek, M., & Conroy, C. 2013, *ApJL*, 775, L16
 Kriek, M., Conroy, C., van Dokkum, P. G., et al. 2016, *Natur*, 540, 248
 Kriek, M., Shapley, A. E., Reddy, N. A., et al. 2015, *ApJS*, 218, 15
 Kriek, M., van Dokkum, P. G., Labbé, I., et al. 2009, *ApJ*, 700, 221
 Kroupa, P. 2001, *MNRAS*, 322, 231
 Lonoce, I., Longhetti, M., Maraston, C., et al. 2015, *MNRAS*, 454, 3912
 Maiolino, R., & Mannucci, F. 2019, *A&ARv*, 27, 3
 Mannucci, F., Cresci, G., Maiolino, R., et al. 2009, *MNRAS*, 398, 1915
 Maoz, D., Mannucci, F., & Brandt, T. D. 2012, *MNRAS*, 426, 3282
 McCracken, H. J., Milvang-Jensen, B., Dunlop, J., et al. 2012, *A&A*, 544, A156
 Momcheva, I. G., van Dokkum, P. G., van der Wel, A., et al. 2017, *PASP*, 129, 015004
 Morishita, T., Abramson, L. E., Treu, T., et al. 2018, *ApJL*, 856, L4
 Mowla, L., van Dokkum, P., Brammer, G., et al. 2018, arXiv:1808.04379
 Muzzin, A., Marchesini, D., Stefanon, M., et al. 2013a, *ApJS*, 206, 8
 Muzzin, A., Marchesini, D., Stefanon, M., et al. 2013b, *ApJ*, 777, 18
 Naab, T., Johansson, P. H., & Ostriker, J. P. 2009, *ApJL*, 699, L178
 Nomoto, K., Thielemann, F.-K., & Yokoi, K. 1984, *ApJ*, 286, 644
 Onodera, M., Carollo, C. M., Renzini, A., et al. 2015, *ApJ*, 808, 161
 Peng, C. Y., Ho, L. C., Impey, C. D., & Rix, H.-W. 2002, *AJ*, 124, 266
 Salpeter, E. E. 1955, *ApJ*, 121, 161
 Scoville, N., Aussel, H., Brusa, M., et al. 2007, *ApJS*, 172, 1
 Shapley, A. E., Sanders, R. L., Reddy, N. A., et al. 2017, *ApJL*, 846, L30
 Thomas, D., Maraston, C., & Bender, R. 2003, *MNRAS*, 343, 279
 Toft, S., Gallazzi, A., Zirm, A., et al. 2012, *ApJ*, 754, 3
 Tomczak, A. R., Quadri, R. F., Tran, K.-V. H., et al. 2014, *ApJ*, 783, 85
 Tremonti, C. A., Heckman, T. M., Kauffmann, G., et al. 2004, *ApJ*, 613, 898
 van Dokkum, P. G. 2001, *PASP*, 113, 1420
 van Dokkum, P. G., Franx, M., Kriek, M., et al. 2008, *ApJL*, 677, L5
 Whitaker, K. E., Kriek, M., van Dokkum, P. G., et al. 2012, *ApJ*, 745, 179
 Wuyts, S., Labbé, I., Franx, M., et al. 2007, *ApJ*, 655, 51
 Yano, M., Kriek, M., van der Wel, A., & Whitaker, K. E. 2016, *ApJL*, 817, L21